JBC Papers in Press. Published on April 27, 2012 as Manuscript M111.320481
The latest version is at http://www.jbc.org/cgi/doi/10.1074/jbc.M111.320481

Loss of the Mammal-Specific Tectorial Membrane Component CEA Cell Adhesion Molecule 16 (CEACAM16) Leads to Hearing Impairment at Low and High Frequencies

Robert Kammerer[1], Lukas Rüttiger[2], Rainer Riesenberg[3], Constanze Schäuble[3], Rosemarie Krupar[3], Annegret Kamp[3], Kishiko Sunami[4], Andreas Eisenried[3, #], Martin Hennenberg[5], Fritz Grunert[6], Andreas Breß[2], Sebastiano Battaglia[7, §], Heinrich Schrewe[7], Marlies Knipper[2], Marlon R. Schneider[8], Wolfgang Zimmermann[3,*]

[1]Instute of Immunology, Friedrich-Loeffler Institut, Greifswald-Insel Riems, Germany; [2]Department of Otorhinolaryngology, University of Tübingen, Hearing Research Centre Tübingen, Tübingen, Germany; [3]Tumor Immunology Laboratory, LIFE Center, University Clinic of Munich, Munich, Germany; [4]Department of Otolaryngology, Osaka City University Medical School, Osaka, Japan; [5]Experimental Urology, Department of Urology, University Clinic of Munich, Munich, Germany; [6] Aldevron Freiburg, Freiburg, Germany; [7] Institute of Medical Genetics - CBF, Charité-University Medicine-Berlin, Berlin, Germany, and Max-Planck Institute for Molecular Genetics, Berlin, Germany; [8]Institute of Molecular Animal Breeding and Biotechnology, Gene Center, University of Munich, Munich, Germany.

[#] Present address: University Erlangen-Nürnberg, Department of Anesthesiology, Erlangen, Germany; § Present address: Department of Pharmacology and Therapeutics, Roswell Park Cancer Institute, Buffalo, NY, USA; *Corresponding author

Running Title: CEACAM16 inner ear function

To whom correspondence should be addressed: Wolfgang Zimmermann, Tumor Immunology Laboratory, LIFE Center, University Hospital of Munich, Ludwig-Maximilians-University Munich, Marchioninistrasse 23, D-81377 Munich, Germany, Tel.: +49 89 7095-4895; Fax; +49 89 7095-4864; Email: wolfgang.zimmermann@med.uni-muenchen.de

Keywords: Carcinoembryonic antigen family, knock-out, hearing, cochlea, tectorial membrane, deafness genes

Background: Molecules evolved in mammals for specialization of hearing.
Results: CEA cell adhesion molecule 16 (CEACAM16) is a structural component of the tectorial membrane and necessary for hearing at low and high frequencies.
Conclusion: CEACAM16 has evolved in mammals to broaden the auditory frequency range.
Significance: Mutation of *CEACAM16* is responsible for human autosomal dominant hearing loss (DFNA4).

SUMMARY

The vertebrate-restricted carcinoembryonic antigen gene family evolves extremely rapidly. Among their widely expressed members, the mammal-specific, secreted *CEACAM16* is exceptionally well conserved and specifically expressed in the inner ear. To elucidate a potential auditory function we inactivated murine *Ceacam16* by homologous recombination. In young *Ceacam16*$^{-/-}$ mice the hearing threshold for frequencies below 10 kHz and above 22 kHz was raised. This hearing impairment progressed with age. A similar phenotype is observed in hearing-impaired members of Family 1070 with non-syndromic autosomal dominant hearing loss (DFNA4) who carry a missense mutation in *CEACAM16*. CEACAM16 was found in interdental and Deiters cells and was deposited in the tectorial membrane of the cochlea between postnatal day 12 and 15, when hearing starts in mice. In cochlear sections of *Ceacam16*$^{-/-}$ mice tectorial membranes were significantly more often stretched out as compared to wild-type mice where they were mostly contracted and detached from the outer hair cells. Homotypic cell sorting observed after ectopic cell surface expression of the carboxy-terminal immunoglobulin variable-like N2 domain of CEACAM16 indicated that

CEACAM16 can interact in trans. Furthermore, Western blot analyses of CEACAM16 under reducing and non-reducing conditions demonstrated oligomerization via unpaired cysteines. Taken together, CEACAM16 probably can form higher order structures with other tectorial membrane proteins such as α-tectorin and β-tectorin and influences the physical properties of the tectorial membrane. Evolution of *CEACAM16* might have been an important step for the specialization of the mammalian cochlea allowing hearing over an extended frequency range.

The carcinoembryonic antigen (CEA) family, a subgroup of the immunoglobulin superfamily, is extremely variable in size and, with few exceptions, exhibits little sequence conservation between species. Phylogenetic analyses provide evidence that the primordial CEA gene family in mammals consisted of five genes, including the immune inhibitory receptor-encoding CEA-related cell-cell adhesion molecule 1 (CEACAM1) ancestor. Most of the heterogeneity of CEA families between different species is derived from members that are closely related to CEACAM1. CEACAM1-related genes can be traced back to the last common ancestor of fishes and mammals (1). CEACAM1 exhibits a wide spectrum of functions including regulation of innate and adaptive immune responses, granulopoiesis, angiogenesis, glucose and fat metabolism, tissue architecture and homoeostasis (2-10). Most significantly from an evolutionary point of view, CEACAM1 in humans, mouse and probably other species is exploited by bacterial and viral pathogens as a receptor to enter the host via mucosal surfaces through interaction with adhesins (11). Once inside the host, the pathogens can gain additional benefit by down-regulation of anti-pathogen immune responses through engagement of CEACAM1 on epithelial and immune cells (8;10;11). This dual level assault has led to the development of very similar decoy receptors during evolution as a countermeasure by the host (1;12;13). Taken together, the struggle to escape from pathogen recognition and generation of decoy receptors are probably responsible for the pronounced diversity and low sequence conservation observed between CEA families of different species (1).

The non-CEACAM1-like primordial members represent a more distantly related group of the CEA family-related genes of unknown function (*CEACAM16, CEACAM18, CEACAM19, CEACAM20*) (14). In contrast to CEACAM1-related genes, for which by sequence comparison alone no orthologous genes can be assigned, orthologs for this CEACAM subgroup were identified in placental mammals, marsupials and in the monotreme platypus (1). In platypus, only CEACAM16 was found. Whereas CEACAM1-related members abound in amphibians and fishes, the group of orthologous CEACAMs appears to be restricted to the mammalian lineage (W.Z. and R.K., unpublished results and (1)). Among them, CEACAM16 sticks out in being exceptionally well conserved and representing the only secreted member with two immunoglobulin (Ig) variable (IgV)-like or N domains, one NH_2-terminal (N1) and one COOH-terminal (N2) separated by 2 Ig constant (IgC)-like domains (A and B). With the exception of the secreted CEACAM1-related pregnancy-specific glycoproteins (PSG), which are found only in certain mammals (1), the vast majority of CEACAMs is membrane bound and in general composed of one N domain followed by a varying number of IgC-like domains. CEACAMs´ N domains are involved in homo- and heterotypic interactions whereby the β-sheet formed by β-strands C´´C´CFG is instrumental for the interaction with their ligands (15;16). Therefore, the domain arrangement of CEACAM16 suggests interaction with two binding partners. Furthermore, CEACAM16 exhibits a very restricted expression pattern. Murine *Ceacam16* was found to be weakly expressed in only one out of 37 adult and embryonic tissues analyzed, i.e. in the cerebellum (14).

As a basis for functional analyses of this mammal-specific, highly conserved member of the CEA family we searched expressed sequence tag (EST) databases for CEACAM16 clones. CEACAM16 ESTs were frequently detected in inner ear cDNA libraries. Immunohistochemistry of *Ceacam16*$^{-/-}$ and wild-type mice cochleae revealed specific expression in the tectorial membrane (TM), thus adding a fifth member to the list of non-collagenous proteins (α-tectorin, β-tectorin, otogelin, otolin) specific to this acellular extracellular matrix. The TM covers the sensory hair cells of the inner ear and translates sound-induced vibrations to shearing of hair cell

stereocilia. Accordingly, the TM is an indispensable component of the mechano-electrical transduction that leads to amplification of sound-induced vibrations of the basilar membrane. Loss of CEACAM16 resulted in an increased hearing threshold mainly for frequencies below 10 kHz and impaired amplification above threshold possibly caused by disruption of the striated-sheet of the TM with concomitant change of its elasticity.

EXPERIMENTAL PROCEDURES

Cell lines and antibodies–HeLa, BOSC23 and HEK293T were cultured in RPMI medium supplemented with 10% fetal bovine serum (FBS Gold; PAA Laboratories GmbH) and 1% penicillin /streptomycin /glutamine at 37°C in a humidified atmosphere and 5% CO_2. The following antibodies were used: polyclonal rabbit anti-α-tectorin antibody (sc-98277; Santa Cruz Biotechnology,), monoclonal mouse anti-c-myc antibody (MCA2200; Serotech), mouse anti-β-actin antibody (clone AC-74; Sigma-Aldrich), rabbit polyclonal anti-prestin/SLC26A5 antibody, rabbit anti-KIR4.1/KCNJ10 antibody, horseradish peroxidase (HRP)-coupled goat anti-mouse immunoglobulin (Ig) (Southern Biotech) and fluorescein-isothiocyanate (FITC)-coupled goat $F(ab')_2$ anti-mouse IgG/IgM from Jackson ImmunoResearch (Dianova). Polyclonal and monoclonal murine anti-murine and anti-human CEACAM16 antibodies were generated by genetic immunization and tested essentially as described before (17). The monoclonal anti-CEACAM16 antibody 9D5 was purified by protein G sepharose affinity chromatography and biotinylated using standard procedures.

RNA isolation and reverse transcription PCR–Human inner ear RNA was isolated from autopsy samples. The use of human autopsy samples of this study was approved by the Ethics Committee of the Medical Faculty of the University of Munich. The temporal bone was collected within 12 h after the subject's death and placed on ice. The oval and the round windows were opened and the cochlea was perfused with RNAlater® (Ambion, Applied Biosystems). The inner ear was microdissected and RNA was isolated using the TRIzol® reagent (Life Technologies). From fresh murine tissue or tissue stored in RNAlater at 4°C RNA was isolated with the RNeasy® Plus Mini Kit including a DNA removal step (Qiagen). Tissues were homogenized in RLT buffer using an Ultraturrax homogenizer (IKA Werke). Mouse cochleae were directly suspended in RLT by crushing the tissue with tweezers. The quality of RNA was analyzed by capillary electrophoresis on an Agilent Bioanalyzer 2100 system using the RNA 6000 Pico Kit (Agilent Technologies). One µg of total murine or human RNA (Chemicon, Millipore GmbH; BioChain Institute) were reverse transcribed using the Reverse Transcription System® (Promega) followed by PCR (25 µl total volume) with one twentieth of the reverse transcription (RT) reaction and gene-specific primers (Supplementary Table 1) using standard conditions. Quantitative RT-PCR was performed using the LightCycler technology (Roche) and gene-specific primers (Supplementary Table 1). Crossing points (Cp) were used to calculate relative mRNA levels present in the RNA samples after β-actin mRNA normalization.

Gene targeting in embryonal stem cells and generation of CEACAM16 null mice–All experiments which involved animals were based on the institutional guidelines of the Universities of Tübingen and Munich and registered and performed in compliance with the German Animal Protection Law (Regierung von Oberbayern and the Regierungspräsidium Tübingen). The targeting vector was constructed by insertion of *Ceacam16* genomic regions comprising exon 1 (5´-region) and part of exon 5 and 6 (3´-region) into the pPTN4 vector (18). *Ceacam16* regions were amplified by PCR (primers see Supplementary Table 1) with BALB/c genomic DNA as template using the Expand High Fidelity^{PLUS} PCR System Kit (Roche Diagnostics).The resulting targeting construct lacks a 6.8 kb region which comprises exons 2-4, and part of exon 5 of *Ceacam16* that was replaced by a 1.7 kb neo cassette. Electroporation of the *Sal*I-linearized targeting vector into the BALB/c-derived ES cell line BALB/c-I (19), G418 selection for recombinants and ES cell propagation were performed as described before (20). Appropriate clones were injected into C57BL/6J blastocysts and these were implanted into a NMRI foster mother. The resulting male chimeras were backcrossed to BALB/c females to identify germ line transmission of the targeted allele and to produce mice heterozygous for the null mutation. F1 intercrosses of heterozygous mice finally resulted

in F2 offspring on pure BALB/c background. *Ceacam16*$^{-/-}$ and *Ceacam16*$^{+/+}$ strains were established and maintained at the animal facilities of Gene Center and the Walter Brendel Center of Experimental Medicine, University of Munich, Germany.

ES cell and mouse genotyping–Homologous recombination between the targeting vector and *Ceacam16* in drug-resistant ES cell clones was analyzed by long range PCR using the Expand Long Template PCR System (Roche) and the EUCOMM Expand Long Template genotyping protocol (http://www.knockoutmouse.org/kb/entry/23/). As a positive control, a vector was created with an extended 5′-targeting region. Southern blotting was performed using *Bam*HI-digested genomic DNA and ^{32}P-labeled hybridization probes applying standard techniques. The established *Ceacam16* knock-out and wild-type strains were genotyped using standard PCR reaction conditions and the primers indicated in Supplementary Table 1.

Hearing measurements–Thirty adult male and female *Ceacam16*$^{-/-}$ and *Ceacam16*$^{+/+}$ mice (6 weeks to 19 months old) were used for hearing tests. Measurements of auditory brainstem responses (ABR) and distortion products of the otoacoustic emissions (DPOAE) were performed as described (21-23) while mice were under ketamine (75 mg/kg body weight) and xylazine (5 mg/kg body weight) anesthesia. In short, ABR to free field click (100 µs), noise burst (1 ms) and pure tone (3 ms, 1 ms ramp) acoustic stimuli were recorded with subdermal silver wire electrodes at the ear (active), the vertex (reference) and the back (ground) of the animals. Signals were amplified (50100-fold), band-pass filtered (200 Hz high-pass and 5 kHz low-pass) and averaged for 64-256 repetitions at each sound pressure level (SPL) presented (0-100 or 0-110 dB in steps of 5 dB). Hearing threshold was defined as the lowest SPL that produced a potential visually distinct from background noise. The cubic 2f1-f2 DPOAE was measured for f2 = 1.24f1 and L2 = L1-10 dB. Emission signals were recorded during sound presentation of 260 ms and averaged four times for each sound pressure (L1 ranging from -10 to 65 dB SPL) and frequency (f2 ranging from 4.0 to 32.0 kHz) presented. Threshold was determined as the L1 sound pressure that could evoke a 2f1-f2 DP signal reliably exceeding 5–10 dB above noise level, with the noise level typically being at -20 dB SPL.

Acoustic trauma was induced with loud sound of binaural exposure to 120 dB SPL band-pass noise (4-16 kHz) in free field. ABR waves from individual ears were measured and analyzed for -10 to +85 dB SPL stimulation level to click stimuli. From averaged ABR waves, the signal derivative was calculated as a measure for the waviness of the curves and presented as input-output (I/O) function. An ABR wave with large positive and negative deflections, i.e. a strong ABR signal, would reflect in a higher signal derivative. A flat curve will have a signal derivative of ca. 0.

Immunohistology–Mice were anesthetized with isoflurane and killed by cervical dislocation. The cochlea and vestibular organ were quickly removed *en bloc*, and fixed for 30-45 min in 4% phosphate-buffered saline (PBS)-buffered formaldehyde at room temperature, rinsed in PBS, decalcified for 24 h in 0.18 M citric acid, 0.44 M EDTA pH 7.1 at 4°C and stored in 70% ethanol at 4°C until embedded in paraffin wax using a Shandon Hypercenter XP Enclosed Tissue Processor (Thermo Scientific). Three to 5 µm thin sections were applied to SuperFrost Ultra Plus® slides (Menzel), heated to 40°C for 0.5 h, dried at room temperature for 2 days, deparaffinized and rehydrated. Antigen retrieval was achieved by heating to ~95°C of the tissue sections in Target Retrieval Solution, pH 9 (DakoCytomation) for 30 min followed by cooling to room temperature for 20 min. After blockage of endogenous peroxidase and biotin by incubation with 3% H_2O_2/10% methanol in PBS for 5 min at room temperature and by using the Streptavidin/Biotin Blocking Kit (Vector Laboratories; Linearis), respectively, sections were reacted with the biotinylated anti-CEACAM16 antibody 9D5 (4 µg/ml) for 2 h at room temperature or over night at 4°C, followed by a 1 h incubation with horseradish peroxidase-coupled streptavidin (Sigma-Aldrich) and stained by incubation with 3-amino-9-ethylcarbazole.

For immunofluorescence staining the cochlea and the vestibular organ were fixed for 2 h in 2% freshly prepared formaldehyde, 125 mM sucrose in 100 mM PBS, pH 7.4 at room temperature followed by overnight incubation with 25% sucrose with 1 mM protease inhibitor Pefabloc SC (Roche Diagnostics) in PBS. Decalcification of cochleae from adult mice was performed using

Rapid Bone Decalcifier medium (Eurobio, Fisher-Scientific) for 15 min to 2 h. Cochleae were embedded in O.C.T. compound (Miles Laboratories). Ten µm cryosections were mounted on SuperFrost Ultra Plus® slides, dried for 1 h and stored at -20°C. Cochlear sections were first treated with 0.5% Triton-X-100 (Sigma-Aldrich) for 10 min and blocked with 7% normal goat serum (Sigma-Aldrich) in PBS for 1 h, followed by overnight incubation with anti-CEACAM16 antibody 9D5 (4 µg/ml) and rabbit polyclonal anti-prestin or rabbit anti-KIR4.1 antibodies at 4°C. Primary antibodies were detected with either Cy3-conjugated goat-anti-rabbit Ig antibody (0.35 µg/ml; Jackson Immuno Research Laboratories) or Alexa-488 conjugated goat-anti-mouse Ig antibody (1:1500; Molecular Probes). Sections were mounted with Vectashield mounting medium containing DAPI (Vector Laboratories) and photographed using the Olympus BX61 microscope with epifluorescence and the cellSens Dimension® Software (Olympus). For all immunohistochemical pictures image stacks along the x-axis (z-stack) and deconvolution were used.

In situ hybridization–Cryosections were prepared as described for immunofluorescence staining. Digoxigenin-tagged sense and antisense riboprobes were transcribed from the pCMV-SPORT6 vector containing the 5′-half of the murine CEACAM16 cDNA. Sections were hybridized with 1:50 diluted riboprobes in 1 x hybridization buffer (Roche Diagnostics) at 64°C over night, washed twice in 0.1% saline-sodium citrate (SSC) buffer, blocked with 1 x Blocking Reagent (Roche Diagnostics) in 100 mM Tris-HCl pH 7.5, 0.3% Triton X-100 (blocking solution). Riboprobes were reacted with alkaline phosphatase-coupled anti-digoxigenin antibodies (Roche Diagnostics) diluted 1:750 in blocking solution for 30 min at 37°C, followed by staining with 5-bromo-4-chloro-3-indolyl-phosphate/nitro blue tetrazolium (Sigma-Aldrich) for 5-20 h. Sections were embedded in Mowiol (Roth) and pictures were taken using a Olympus AX70 microscope.

Generation of CEACAM16 expression vectors–Full length murine and human CEACAM16 were amplified from total cochlear RNA and *stria vascularis* RNA, respectively, after reverse transcription (see above) using primers located in the 5′- and 3′-untranslated regions (Supplementary Table 1) and High Fidelity PCR Enzyme Mix (Fermentas) and cloned into the vector pCMV-SPORT6 (sequences were deposited at GenBank with accession numbers NM_001039213; NM_001033419). For identification of the domains responsible for homophilic interaction of CEACAM16, intermolecular disulfide bridge formation and binding with monoclonal antibody, deletion constructs were generated in the VV1, pB1 (Aldevron Freiburg) and pAPtag-5 vectors (GeneHunter Corporation, Nashville, TN, USA) which allow the expression of recombinant proteins with N-terminal or C-terminal myc tags. VV1 and pB1 also provide a C-terminal signal sequence for glycosylphosphatidyl inositol (GPI) anchorage. Addition of a stop codon in front of the GPI signal yielded secreted proteins.

Cell adhesion assay–HEK293T cells (2 x 10^5 cells/6-well plate well) were transiently transfected with 2 µg of VV1, pB1 or pAPtag-5 expression plasmids and 3 µl of FuGENE 6 in 1 ml of media. After 48 h cells were harvested by pipetting, washed in PBS and resuspended by repeated pipetting in 2.5 ml of PBS at room temperature to form a single cell suspension (0.625 x 10^6 cells/2.5 ml). To some samples with high transfection efficiency half of the cells were replaced with non-transfected HEK293T cells to adjust the fraction of CEACAM16-expressing cells to ~50% in order to visualize homotypic cell aggregation. The cell suspensions were slowly rotated or repeatedly gently mixed to prevent sedimentation of the cells for 30-60 min. One hundred µl of the cell suspension were pelleted onto glass slides (SuperFrost Plus®) using a cytocentrifuge (Shandon). The slides were dried for 12-18 h at room temperature and stored at -20°C. After fixation in acetone and blockage of endogenous peroxidase as described above, cells were incubated with 2 µg/ml mouse anti-human CEACAM16 9D5 or 10 µg/ml mouse anti-c-myc antibody. Bound antibodies were visualized using the ImmPRESS anti-mouse Ig kit (Vector Laboratories). The size of aggregates consisting of CEACAM16-expressing cells was determined using a microscope fitted with a graded ocular. Expression levels of CEACAM16 domains on HEK293T cells were quantified after incubation with anti-c-myc antibody (100 µg/ml) followed by FITC-coupled goat anti-mouse Ig antibody (75 µg/ml) using FACScan analysis (FACSCalibur, BD).

Structure prediction–The three dimensional structures of CEACAM16 was modeled using the Geno3D-release 2 homology modeling software (15;24). For modeling of the entire CEACAM16 molecule we selected human CEA (pdb 1E07) as a template. Individual Ig domains were modeled by selecting the following templates: pdb2qsqA-0 and pdb1l6zA-0 for CEACAM16 N1 and CEACAM16 N2; pdb1l6zA-0 for CEACAM16 A; pdb1cs6A-2 and pdb2om5A-0 for CEACAM16 B.

Western blot analysis–HEK293T cells were transiently transfected with expression constructs encoding GPI-linked or secreted CEACAM16 domains as described above. $1x10^6$ cells were dissolved in 100 µl of lysis buffer (50 mM Tris-HCl, 150 mM NaCl, 1% Triton X-100, pH 8, protease inhibitor cocktail [Complete Mini; Roche]) on ice, sonicated briefly, vortexted, centrifuged at 20,800x g for 30 min at 4°C and stored at -20°C. The cell culture supernatant (with 5% FBS) of cells transfected with expression constructs for secreted CEACAM16 variants was centrifuged as above and stored at -20°C. After addition of sodium dodecyl sulfate (SDS) sample buffer (without 2-mercaptoethanol) samples were heated in the presence or absence of 60 mM dithiothreitol for 10 min at 95 °C, and stored at -20 °C until Western blot analyses were performed. Samples (corresponding to 5 µl of lysate) were separated by electrophoresis on 8 or 12% polyacrylamide gels containing SDS and blotted onto nitrocellulose membranes. Membranes were blocked over night in PBS with 0.1% Tween 20 (Roth) (PBS-T), containing 5% blotting-grade milk powder (Roth). Antigen detection was performed using anti-CEACAM16 (5 µg/ml), anti-c-myc (1.6 µg/ml) or anti-β-actin antibodies (2.5 µg/ml) in PBS-T with 5% milk powder. Subsequently, membranes were washed with PBS-T, and incubated with secondary peroxidase-coupled antibodies (Calbiochem, San Diego, USA) diluted 1:4000 in PBS-T with 5% milk powder. Blots were developed with enhanced chemiluminescence using ECL Hyperfilm (GE Healthcare).

Statistics–Data are presented as mean and standard deviation (SD) or mean and standard error of the mean (SE). Differences of the mean were compared for statistical significance by 2-way ANOVA (GraphPad Prism 2.01) and Student's t-test. Statistical significance was tested at alpha = 0.05. The two-sided Fisher's exact test was used for contingency testing.

RESULTS

CEACAM16 is selectively expressed in the inner ear–A survey of expressed sequence tag (EST) databases revealed that 80% of a total of 57 Ceacam16 cDNAs originated from adult inner ear or organ of Corti (Supplementary Fig. 1A) which suggested preferential expression of CEACAM16 in inner ear tissue. This was corroborated by the analysis of CEACAM16 transcripts by PCR amplification using gene-specific primers after reverse transcription of a panel of 22 human tissues, including brain and pituitary which in mice were found to contain low levels of Ceacam16 mRNA (see below). CEACAM16 mRNA was detected in none of the tissues (Supplementary Fig. 1B). However, a strong signal was found for total RNA from murine cochleae (Fig. 1A). The presence of more than 100-fold lower levels of *Ceacam16* transcripts could also be demonstrated in cerebellum and pituitary (Fig. 1A, B). In dissected adult human inner ears (Fig. 1C) CEACAM16 transcripts could be detected in lateral wall preparations but not in other parts of the cochlea (organ of Corti, spiral ganglia) or in the vestibular organ (anterial and horizontal ampulla, utricle).

Young Ceacam16$^{-/-}$ mice have increased hearing threshold for pure tones and a limited outer hair cell amplification force–The restricted expression of the *Ceacam16* gene in the cochlea prompted us to asses whether inactivation of *Ceacam16* would impair hearing in mice. To this end we deleted exons 2, 3, 4 and part of exon 5 including its splice acceptor site in BALB/c embryonic stem (ES) cells by homologous recombination which should lead to a *Ceacam16* null allele (Fig. 2A). To identify clones with putative homologous recombination events we used long range PCR and primers in the neo gene and in the 5´-upstream region distal to the genomic fragment present in the targeting vector. Three out of 200 G418-resistant ES cell clones yielded a fragment with the expected size (Fig. 2B and data not shown). Southern blot analysis using a unique probe downstream of the 3´-targeting region revealed the presence of the expected 8.2 kb genomic fragment after *Bam*HI digestion suggesting correct homologous recombination events in all three ES cell clones (Fig. 2C, left

panel). Clone C3 was injected into C57BL/6 blastocysts to generate chimeric mice that were back-crossed to BALB/c mice. Albino mice which carried the null allele were mated to obtain *Ceacam16*$^{-/-}$, *Ceacam16*$^{+/-}$ and *Ceacam16*$^{+/+}$ mice. The frequencies of the resulting genotypes were close to the expected Mendelian ratio (25.3 : 42.1 : 32.6; n = 95). No sex bias was observed (*Ceacam16*$^{-/-}$ male/*Ceacam16*$^{-/-}$ female = 13 : 12). Southern blot analysis using a probe from the 5′-upstream region (Fig. 2A) confirmed correct homologous recombination in mice derived from ES cell clone C3 (Fig. 2C, right panel). *Ceacam16*$^{-/-}$ mice are fertile and the mean litter size (± standard deviation) is lower than that of wild-type matings but the difference does not reach significance (4.1 ± 1.6, n = 11; 5.7 ± 1.9, n = 9; p = 0.086, Mann-Whitney U test). No corresponding mRNA and protein could be detected in cochleae of *Ceacam16*$^{-/-}$ mice (Fig. 2D, E).

To assess the loss of CEACAM16 on the hearing function, we studied young *Ceacam16*$^{+/+}$ and *Ceacam16*$^{-/-}$ mice (1-2 month old) by recording auditory brainstem responses (ABR) and distortion products of the otoacoustic emissions (DPOAE). ABR hearing threshold with click stimuli were not found to be significantly different (Fig. 3A), indicating that wild-type and *Ceacam16*$^{-/-}$ mice still had a similar 'best hearing' at this young age. In the low and high frequencies of the hearing range threshold were significantly increased in *Ceacam16*$^{-/-}$ mice (Fig. 3B), indicating impaired auditory signal transduction in the cochlea at frequencies towards the borders of the hearing range (2-8 kHz and >22 kHz), where higher stimulation levels are needed to evoke an ABR response (>40 dB SPL). This threshold loss was not seen by stimulation with the multi-frequency click stimulus (Fig. 3A), that coincidentally excites multiple parts of the cochlea and is a measure for the 'best threshold response'. However, single ears of *Ceacam16*$^{-/-}$ mice appear to have already increased threshold (Fig. 3A, open circles) but differences are not quite significant (p = 0.08). Nevertheless, ABR waveform analysis for suprathreshold stimulation could disclose reduced signal strength (Fig. 3C, upper panel, amplitude) and 'waviness' (Fig. 3C, lower panel, derivative) in brainstem responses. To find out whether the origin of the hearing loss is based on a sensory-neural hearing loss by impaired inner hair cells (IHC), synaptic transmission, or spiral ganglion (SG) neuron malfunction, or rather a deficit in the active amplification process in the cochlea by outer hair cells (OHC) motility, DPOAE functions were studied. DPOAE signals to a stimulus level of 50 dB SPL (L1) is a measure for the optimum (max) amplification by OHCs. One to 2 month old *Ceacam16*$^{-/-}$ mice had a significantly reduced 2f1-f2 DPOAE amplitude at this stimulation level (Fig. 3D), indicating the reduction of the force coupled into the cochlear amplifier by OHC motility. On the other hand, threshold SPL for evoking DPOAE signals were not found to be significantly different (Fig. 3E, p = 0.163, 2-way ANOVA). This was also reflected in the growth of the DPOAE signal with increasing stimulus level L1 (Fig. 3F, shown for 11.3 kHz): while the threshold for 2f1-f2 signal in both *Ceacam16*$^{+/+}$ and *Ceacam16*$^{-/-}$ mice was not significantly different, growth of 2f1-f2 dropped behind in *Ceacam16*$^{-/-}$ mice at suprathreshold stimulation levels, indicating reduced force coupling into the cochlear amplifier over the whole suprathreshold sound pressure range.

Aged Ceacam16$^{-/-}$ *mice have impaired hearing for click-, noise-, and pure tone-stimuli, and have reduced cochlear amplification*– Auditory function is subject to age-related changes (age-related hearing loss). To study the importance of the CEACAM16 protein for the maintenance of hearing function in advanced age, we measured ABR and DPOAE functions in *Ceacam16*$^{+/+}$ and *Ceacam16*$^{-/-}$ mice at the age of 7-19 months. ABR threshold was examined with click, noise burst, and frequency-specific tone burst stimuli in 10 aged *Ceacam16*$^{-/-}$ mice (Fig. 3G-L). The threshold was significantly increased in *Ceacam16*$^{-/-}$ mice for click (Fig. 3G), noise burst (not shown) and frequency-specific stimuli of 2-8 kHz stimulation frequency (Fig. 3H). From the ABR threshold, the loss of hearing function that has been found already in young mice exclusively by frequency-specific stimulation (compare Fig. 3B), now manifests also with click and noise burst stimulation because the threshold for 'best hearing' frequencies was also affected.

ABR waveform amplitudes were reduced and latencies were prolonged by age (Fig. 3I, upper panel) and ABR waveform deflections ('waviness' as a function of stimulus level (dB SPL) was reduced by age-related hearing loss in wild-type

and knock-out animals (compare Fig. 3C and Fig. 3I, lower panel).

The DPOAE functions (Fig. 3J-L) confirm an age related reduction in 2f1-f2 amplitude in both, wild-type and knock-out mice (compare Fig. 1D, J) and show the reduced cochlear amplification also in aged mice. The DPOAE threshold, not significantly different between young wild-type and knock-out mice (Fig. 3E), has become significantly affected in aged *Ceacam16*$^{-/-}$ mice as compared to wild-type mice, seen by the 2f1-f2 growth function for 11.3 kHz stimulation (Fig. 3L) and the DPOAE threshold audiogram (Fig. 3K). In conclusion, the hearing deficits described in young *Ceacam16*$^{-/-}$ mice were found also in aged mice, with a higher degree of obviousness in the OHC amplification-based DPOAE threshold function.

Ceacam16$^{-/-}$ *mice are not more vulnerable to noise exposure than age-matched littermate wild-type mice*–The relevance of CEACAM16 protein for the functional resistance against noise overexposure and for the maintenance of normal auditory function after noise induced cochlea trauma was examined by exposing mice to loud sound of 4-16 kHz band noise, 120 dB SPL root-mean-square for 1 h. Hearing function was monitored by ABR and DPOAE measurements before, and 6 days following noise exposure. Noise overexposure leads to permanent sensory trauma on the IHC level (loss of ABR threshold) and on the OHC level (loss of DPOAE threshold and amplitude). *Ceacam16*$^{-/-}$ mice had a similar or even smaller loss of auditory function as compared to *Ceacam16*$^{+/+}$ mice (Supplementary Fig. 2): loss of ABR threshold for click stimuli (Supplementary Fig. 2A) was not significantly different from wild-type mice and loss of threshold for frequency specific stimuli was similar in the high frequency range as compared to wild-type mice (Supplementary Fig. 2B) and was even significantly smaller in the low frequency range. The smaller loss can be explained by the already increased threshold for frequency-specific stimuli in *Ceacam16*$^{-/-}$ mice. Supplementary Fig. 2C, D show a similar profile for the damage on the OHC level: the loss of suprathreshold 2f1-f2 signal strength was significantly smaller in *Ceacam16*$^{-/-}$ mice than in *Ceacam16*$^{+/+}$ mice (Supplementary Fig. 2D). The loss of DPOAE threshold was smaller in *Ceacam16*$^{-/-}$ mice than in wild-type mice, even though the initial 2f1-f2 DPOAE threshold was similar between both genotypes before noise exposure (Fig. 3E). Taken together, the slightly hearing impaired phenotype of *Ceacam16*$^{-/-}$ mice, that was mainly based on the reduced function of OHC amplification, led to reduced vulnerability of OHC function and less ABR threshold loss following noise exposure.

Age-related progression of hearing threshold loss affects Ceacam16$^{-/-}$ *and Ceacam16*$^{+/+}$ *mice in a similar way*–With increasing age, threshold for click ABR stimuli increased in both *Ceacam16*$^{-/-}$ and *Ceacam16*$^{+/+}$ mice (Fig. 4) in parallel (Pearson correlation coefficient: $p < 0.001$) with a 10 dB higher threshold in Ceacam16$^{-/-}$ mice.

CEACAM16 is a structural component of the TM in the organ of Corti and of the macula-associated matrix of the vestibular organ–The type of hearing deficit observed in *Ceacam16*$^{-/-}$ mice suggested an involvement of the TM, an acellular sheet of matrix that runs along the length of the cochlea. It is attached to the spiral limbus, spans the spiral sulcus and covers the organ of Corti with its sensory hair cells. To be able to investigate the distribution of CEACAM16 in the inner ear we generated a monoclonal anti-CEACAM16 antibody which binds to the IgC type A domain of both murine and human CEACAM16 (Supplementary Fig. 3). Immunohistology with this biotinylated monoclonal antibody revealed strong staining of the whole TM from the base to the helicotrema of the cochlea of adult wild-type mice (Fig. 5A, and data not shown). No other structure was consistently stained in the adult wild-type cochlea in comparison to the cochlea of *Ceacam16*$^{-/-}$ mice. In addition, the otolith-containing acellular gel overlying the macula of the saccule was also strongly stained (compare Fig. 5C and 5G). The saccule registers information about linear movements in the vertical plane. Besides in the extracellular matrices of the cochlea and the saccule CEACAM16 was found by immunohistology in interdental cells, Deiters cells and possibly in OHC (Figure 5I, J and K; Fig. 6G, I, J, L). Double-staining using fluorescently labeled anti-CEACAM16 antibodies and antibodies specific for prestin/KCNJ10, an OHC marker, ruled out the presence of CEACAM16 in OHC of adult P49 *Ceacam16*$^{+/+}$ mice (Fig. 7D-F). Using KIR4.1/SCL26A5-specific antibodies which label Deiters cells and pillar cells but not OHC confirmed the presence of CEACAM16 in Deiters cells (Fig. 7A-C). Interestingly, CEACAM16 seems to be present in vesicular structures in the

body as well as in the projections of Deiters cells and appears to reach into the reticular lamina which covers the cells of the organ of Corti (Fig. 7C, I). Inner hair cells (IHC) as well as pillar cells were stained at the apical end (Fig. 7G, H). In cochlear sections of *Ceacam16*$^{-/-}$ mice, no staining with the CEACAM16 antibody was observed (Fig. 7A, inset). *In situ* hybridization of cochlea from young rats (P12) with a Ceacam16 antisense probe confirmed expression of *Ceacam16* in Deiters cells, interdental cells of the limbus and to a lesser degree in phalangeal, inner pillar cells and possibly in inner hair cells in a phylogenetically closely related species (Fig. 8A-C). No other structures were stained in the inner ear including the utricle and the labyrinth (data not shown). We noticed that in adult wild-type mice the TM was often detached from the OHC and more contracted in comparison to the TM in *Ceacam16*$^{-/-}$ mice (compare Fig. 5B, F for example). This difference between wild-type and *CEACAM16*$^{-/-}$ mice was statistically significant ($p = 0.0003$; Fisher's exact test; WT, number of cochleae $n = 8$; KO, $n = 7$; Fig. 5L). No gross abnormality of the distribution of α-tectorin, one of the major protein components of the TM, was seen in *Ceacam16*$^{-/-}$ mice (compare Fig. 5D and 5H). Therefore, deposition of α-tectorin into the tectorial membrane is not perturbed by the absence of CEACAM16.

CEACAM16 is deposited late during TM development–Deposition of proteinacious components of the TM starts already prenatally at about embryonic day (E) 14 in mice (25). Maturation of the TM is observed around postnatal day 15 (P15) a time point in development where mature mechanical and electrical cochlear responses are observed (26). The major components of the TM comprise three types of collagen (collagen II, IX, XI), α-tectorin and β-tectorin, the most abundant non-collagenous proteins as well as otogelin and otolin (27;28). Transcription of the various tectorial proteins can occur in various cell types, and their temporal expression pattern differs (e.g., *Tecta* transcription ceases at P15) (29). To learn more about the possible functional interplay of CEACAM16 with other components of the TM we determined its spatio-temporal expression pattern in the organ of Corti in young mice (P5-P18) at the protein and RNA level. Immunohistological analyses revealed that CEACAM16 could not be detected in P5, P8, and P10 cochleae (compare Fig. 6A-C with Fig. 6D-F). However, at P12 and occasionally at P15, CEACAM16 was found in both the limbal zone and in the marginal band of the TM whereas in the medial zone only the sulcus proximal side of the TM was stained (Fig. 6G, J). At P18 and often already at P15, the TM exhibited homogenous staining for CEACAM16 (Fig. 6H, K; Fig. 6I, L). Despite the presence of background staining in some samples, comparison of wild-type sections with sections from *Ceacam16*$^{-/-}$ mice stained in parallel suggests that both interdental cells and Deiters cells and possibly OHC might be the source of the CEACAM16 protein (compare Fig. 6G, H, I with Fig. 6J, K, L). Quantitation of *Ceacam16* and *Tecta* transcripts by qRT-PCR analyses demonstrated persistent transcriptional activity of *Ceacam16* from P12 into adulthood and an inverse temporal expression activity of *Tecta* (Fig. 6M). In contrast, the stereocilin gene (*Strc*) is only marginally expressed in the cochlea during the developmental time frame investigated (Fig. 6M).

Homotypic interactions of CEACAM16–We had noticed during characterization of the anti-CEACAM16 antibodies where we used transient transfection to express GPI-anchored CEACAM16 on the cell surface to screen sera and hybridoma supernatants by a cell-based ELISA that single-cell suspensions of HEK293T cells expressing GPI-anchored CEACAM16 aggregated homotypically whereas cells expressing native CEACAM16 did not (Fig. 9A-C). These findings suggested that CEACAM16 molecules might interact in an antiparallel fashion also under physiological conditions possibly involving the N1 or N2 domain. Such IgV-like domains are known to be instrumental for homo- and heterophilic interaction of CEACAM family members (30). To test this we expressed N1 and N2 domains separately via a GPI anchor on the cell surface of HEK293T cells by transient transfection and analyzed single cell suspensions for their propensity to aggregate. Although the fraction of cells expressing high levels of N1 (38%) was higher than that observed for N2 transfectants (24%) (Fig. 9D, E, right panels) the N2 transfectants formed more and larger N2-expressing cell aggregates in the presence of 50% untransfected cells added to the aggregation assay (Fig. 9D-F). Notably, no aggregates >9 cells were observed for N1 transfectants whereas 38% of N2-expressing cells were contained in such aggregates

(not shown). This suggests that the N1 domain exhibits a weaker homophilic interaction (if any) than the N2 domain.

Furthermore, we wanted to know whether the phylogenetically highly conserved unpaired cysteine residues in the B and N2 domains (Supplementary Fig. 4) would be suitable to support oligomerization of CEACAM16. To this end we modeled the Ig-like domains of human CEACAM16. Cys-253 and Cys-294 of the B domain were predicted to be located inside of the domain in close proximity thus allowing intra-domain disulfide bridge formation while Cys-239 and Cys-258 are predicted to emerge from the surface possibly allowing oligomerization in cis and/or in trans (Supplementary Fig. 5A, B). In the N2 domain, however, Cys-387 appears to be located in a depression thus seems to less likely allow intermolecular disulfide bond formation (Supplementary Fig. 5C, D). To test the hypothesis we expressed full-length murine CEACAM16 transiently on HEK293T cells. Western blot analysis of cell extracts and cell culture supernatants revealed that in the absence of the disulfide reducing agent dithiothreitol (DTT) CEACAM16 dimers and oligomers could be detected which, however, disappeared upon heating with DTT and were converted to monomers (Fig. 9G). Dimers were also observed in the supernatants when deletion constructs lacking the N2 or both the N1 and the A domain were used (Fig. 9H, J). As expected, a C-terminally truncated CEACAM16 consisting of N1 and A with no unpaired cysteines did not form dimers (Fig. 9K). This indicated that CEACAM16 can dimerize via intermolecular disulfide bonds between B and/or N2 domains also in the absence of the N1 and A or the N2 domain. Similar dimer and oligomer formation were observed in cell extracts when full length or CEACAM16 deletion mutants were ectopically expressed on the cell surface via a GPI anchor which probably supports parallel interaction on the membrane (data not shown). To test whether the single cysteine in the N2 domain can form a disulfide bridge between two N2 domains, we analyzed HEK293T cells expressing secreted or GPI-linked N2 or N1 domains. The latter has no cysteine and served as a negative control. As expected no dimers were observed for N1, whereas higher molecular weight molecule species were observed for the GPI-linked N2 domain which disappeared upon DTT treatment (Fig. 9I, lower and middle panels). Dimers could be seen neither in cell extracts nor supernatants when soluble N2 domains were expressed (Fig. 9I, upper panel and data not shown). These data together with the observation that N2 can support cell adhesion when ectopically expressed on the cell membrane (Fig. 9E, F) indicate that N2 can interact in cis and trans but possibly can form a disulfide bridge only when parallelly aligned.

DISCUSSION

With the conquest of land by formerly aquatic vertebrates, adaptation to the new medium air included development of the cochlear auditory system. Highly complex sensory structures evolved (i.e. the organ of Corti) probably from the vestibular system (31). This organ consists of inner and outer hair cells sandwiched between specialized extracellular matrices namely the basilar membrane and the TM. Hair cells sense the sound-induced vibrations of the basilar membrane. Inner hair cells transmit this information to the central nervous system via auditory nerves. Outer hair cells transform their vibrational stimulation via a voltage-dependent molecular motor into length changes and possibly also stereociliar motion which together with the TM as a physical support help to amplify the basilar membrane motion. In mammals, this amplification mechanism increases the sensitivity of hearing by up to 50-60 dB (32).

From our studies of *Ceacam16*$^{-/-}$ mice we conclude that the mammal-specific CEA family member CEACAM16 is involved in hearing. In *Ceacam16*$^{-/-}$ mice hearing is impaired already at a young age (~ 4 weeks old). This impairment is reflected by an increased hearing threshold for low and high frequency pure tone stimuli and reduced cochlear amplification which is likely to result from a reduced mechanical force within the cochlea rather than a sensory-neural hearing loss. This loss is maintained over a long period of the lifespan, when age-related sensory-neural hearing loss additionally affects the threshold in knock-out and in wild-type mice (Fig. 4). Noise exposure led to somehow smaller loss of hearing function in *Ceacam16*$^{-/-}$ mice as compared to the loss in *Ceacam16*$^{+/+}$ mice, indicating that vulnerability to cochlear trauma is not increased by loss of the CEACAM16 protein in the cochlea. In contrast, a reduced mechanical coupling of OHC motility into

the cochlear amplifier under normal conditions improving detection of close threshold auditory stimuli may account for the reduced noise vulnerability in *Ceacam16*$^{-/-}$ mice.

This is corroborated by a recent publication where it was shown that affected individuals of an American family (1070) with non-syndromic autosomal dominant hearing impairment (DFNA4) progressing during adulthood to ~50 dB, carry a missense mutation in the *CEACAM16* gene (33). The phenotype of affected individuals is very similar to that observed for *Ceacam16*$^{-/-}$ mice. Thus our study adds evidence that the DFNA4 mutation is indeed the cause of this specific hearing impairment in humans and probably leads to loss of function of CEACAM16. The non-syndromic nature of CEACAM16 mutations in humans and mice are explained by the highly restricted expression of CEACAM16 mRNA in the cochlea in both species (Fig. 1, Supplementary Fig. 1). No obvious phenotypes relating to the trace amounts of *Ceacam16* mRNA found in the cerebellum and pituitary of mice were observed.

The type of hearing impairment in *Ceacam16*$^{-/-}$ mice is reminiscent of the phenotype observed for mice with *Tecta* and *Tectb* functional null mutations. *Tecta* and *Tectb* encode the inner ear-specific proteins α-tectorin and β-tectorin, major non-collagenous proteins of the otoconial membrane and TM. Loss of low frequency hearing has been reported for *Tectb* null mice (< 20 kHz) (34). Furthermore, mice with a *Tecta* functional null mutation (*Tecta*$^{\Delta ENT/\Delta ENT}$) similarly exhibit an increased compound action potential (CAP) threshold preferentially at lower frequencies (35). Indeed, CEACAM16 protein could also be detected in the acellular matrices of the cochlea and the saccule i.e. the TM and the otolith-containing acellular gel, respectively. OHC-supporting cells (Deiters cells) as well as interdental cells in the limbus region appear to be the source of CEACAM16 protein production in young mice (Fig. 5, 6). In adult mice (P49) cell-associated CEACAM16 could be unequivocally identified in Deiters cells as well as in pillar cells and inner hair cells from where CEACAM16 is possibly released via the Deiters cells projections and reaches the TM by diffusion (Fig. 7). This apparently contradicts findings of Zheng *et al.* who detected *Ceacam16* transcripts in OHC by *in situ* hybridization in 42 days old mice (33). This can possibly be explained by visual overlap of OHC and Deiters cell compartments in the *in situ* experiment of Zheng et al. (33). Indeed, we could demonstrate the presence of Ceacam16 transcripts in Deiters cells, interdental cells, pillar cells and possibly in inner hair cells by *in situ* hybridization using sections cut in parallel to the outer hair cell-Deiters cell axis (Fig. 8). In addition, our data demonstrate that, in comparison to α-tectorin, CEACAM16 protein is deposited in the TM rather late during development of the inner ear. α-tectorin mRNA amounts in the cochleae drop rapidly after birth reaching baseline levels in P15 mice, a time point where peak levels of CEACAM16 mRNA were observed (Fig. 6M) (29). This might explain the finding that in mice at hearing onset (P14-P15) a higher CAP threshold is observed (26) which could be due to TM immaturity caused by incomplete deposition of CEACAM16 in the TM at this time of development. CEACAM16 appears to be evenly distributed not until an age of P15-P18 (Fig. 6). In contrast to *Tecta, Ceacam16* transcription continues into adulthood. Besides continued expression in Deiters cells CEACAM16 production is possibly shifted in adult mice to cells in the lateral wall (e.g. *stria vascularis*) and secreted into the endolymph as suggested by the presence of CEACAM16 mRNA in human lateral wall preparations (Fig. 1). This, however, could not be corroborated by *in situ* hybridization experiments using adult mouse cochleae (data not shown). Therefore, this discrepancy regarding CEACAM16 expression in mouse and humans remains unresolved and still has to be clarified.

CEACAM16 was suggested to represent the link structure within the TM which connects α-tectorin, to which CEACAM16 binds, with the tip of the stereocilia (33). Participation of α-tectorin in the linkage of the TM to the stereocilia was postulated by Legan and coworkers, since in *Tecta*$^{\Delta ENT/\Delta ENT}$ functionally null mice complete detachment of the TM from the organ of Corti is observed (35). If CEACAM16 were the postulated bridging partner connecting α-tectorin with the suggested counterpart stereocilin on the stereocilia (36), *Ceacam16*$^{-/-}$ mice should have the same phenotype as *Tecta* mutant mice with respect to attachment of the TM to the stereocilia. To the contrary, in *Ceacam16*$^{-/-}$ mice the TM seems to be often connected to the organ of Corti specifically to the OHC (see Fig. 5F, H). Furthermore, stereocilin is detected in the tallest row of stereocilia of OHC by P7 (36), a time point in

development when stereocilia become associated with the TM and stereocilin deposition on the TM is observed (36). At this time CEACAM16 is still absent from the murine TM (Fig. 6).

Based on our data we rather suggest that CEACAM16 is part of the striated-sheet structure. The detachment of the TM from the OHC in wild-type but not in *Ceacam16*$^{-/-}$ mice during preparation and fixation of the cochlea suggests that CEACAM16 might be involved in the generation of TM elasticity (Fig. 5). The TM is composed of two main structural components: thick radially arranged 20 nm fibrils made of collagens II and IX which are embedded in a finely striated-sheet matrix composed of about 7 nm wide alternating dark and light fibrils with a repeat width of 30-46 nm (37). α-tectorin and β-tectorin but not otogelin, an additional noncollagenous component of the TM, are essential for the formation of the striated-sheet matrix since lack of expression of the former two proteins leads to loss of an organized striated-sheet matrix (34;35;38). Since there is convincing evidence that CEACAM16 interacts with α-tectorin (33) and probably can form oligomers via homophilic interaction stabilized by disulfide bridges (Fig. 9) it can be envisaged that CEACAM16 is part of the striated-sheet matrix and forms possibly the darker of the two discernible fibrils and the much longer α-tectorin together with β-tectorin possibly by interaction via their *zona pellucida* (ZP) domains, known as protein polymerization domains (39), the lighter fibril with emanating staggered cross-bridges (Supplementary Figure 6). This is also in agreement with the observed sensitivity of the striated-sheet matrix toward disulfide bridge-disrupting agents (37).

The TM ultrastructure of mammals differs from that of birds (31). Interestingly, in addition to collagens II and IX, the striated-sheet matrix within the TM is not found in chickens and thus appears to be restricted to the mammalian lineage. This coincides with the restriction of *CEACAM16* but not *TECTA* and *TECTB* genes to mammals. Since the mammalian basilar membrane extended in length and decreased in width in order to increase the frequency range, appearance of CEACAM16 and mammal-specific collagens in the TM during evolution may have provided the correct physical properties to the TM that it can amplify the motion of the basilar membrane at its characteristic resonance frequencies and thus enhance the sensitivity of mammalian hearing (31).

REFERENCES

1. Kammerer, R. and Zimmermann, W. (2010) *BMC Biol.* **8,** 12
2. Kammerer, R., Stober, D., Singer, B. B., Obrink, B., and Reimann, J. (2001) *J. Immunol.* **166,** 6537-6544
3. Leung, N., Turbide, C., Balachandra, B., Marcus, V., and Beauchemin, N. (2008) *Oncogene* **27,** 4943-4953
4. Gerstel, D., Wegwitz, F., Jannasch, K., Ludewig, P., Scheike, K., Alves, F., Beauchemin, N., Deppert, W., Wagener, C., and Horst, A. K. (2011) *Oncogene* **30,** 4275-4288
5. Lee, S. J., Heinrich, G., Fedorova, L., Al-Share, Q. Y., Ledford, K. J., Fernstrom, M. A., McInerney, M. F., Erickson, S. K., Gatto-Weis, C., and Najjar, S. M. (2008) *Gastroenterology* **135,** 2084-2095
6. Li, C., Chen, C. J., and Shively, J. E. (2009) *Exp. Cell Res.* **315,** 1225-1233
7. Pan, H. and Shively, J. E. (2010) *Immunit.* **33,** 620-631
8. Gray-Owen, S. D. and Blumberg, R. S. (2006) *Nat. Rev. Immunol.* **6,** 433-446
9. Lee, H. S., Ostrowski, M. A., and Gray-Owen, S. D. (2008) *J. Immunol.* **180,** 6827-6835
10. Slevogt, H., Zabel, S., Opitz, B., Hocke, A., Eitel, J., N'guessan, P. D., Lucka, L., Riesbeck, K., Zimmermann, W., Zweigner, J., Temmesfeld-Wollbrueck, B., Suttorp, N., and Singer, B. B. (2008) *Nat. Immunol.* **9,** 1270-1278
11. Kuespert, K., Pils, S., and Hauck, C. R. (2006) *Curr. Opin. Cell Biol.* **18,** 565-571
12. Pils, S., Gerrard, D. T., Meyer, A., and Hauck, C. R. (2008) *Int. J. Med. Microbiol.* **298,** 553-560
13. Sarantis, H. and Gray-Owen, S. D. (2007) *Cell Microbiol.* **9,** 2167-2180
14. Zebhauser, R., Kammerer, R., Eisenried, A., McLellan, A., Moore, T., and Zimmermann, W. (2005) *Genomics* **86,** 566-580
15. Tan, K., Zelus, B. D., Meijers, R., Liu, J. H., Bergelson, J. M., Duke, N., Zhang, R., Joachimiak, A., Holmes, K. V., and Wang, J. H. (2002) *EMBO J.* **21,** 2076-2086
16. Obrink, B. (1991) *Bioessays* **13,** 227-234
17. Kammerer, R., Riesenberg, R., Weiler, C., Lohrmann, J., Schleypen, J., and Zimmermann, W. (2004) *J. Pathol.* **204,** 258-267
18. Conrad, M., Brielmeier, M., Wurst, W., and Bornkamm, G. W. (2003) *Biotechniques* **34,** 1136-8, 1140
19. Noben-Trauth, N., Kohler, G., Burki, K., and Ledermann, B. (1996) *Transgenic Res.* **5,** 487-491
20. Finkenzeller, D., Fischer, B., Lutz, S., Schrewe, H., Shimizu, T., and Zimmermann, W. (2003) *Mol. Cell Biol.* **23,** 272-279
21. Knipper, M., Zinn, C., Maier, H., Praetorius, M., Rohbock, K., Kopschall, I., and Zimmermann, U. (2000) *J. Neurophysiol.* **83,** 3101-3112
22. Schimmang, T., Tan, J., Muller, M., Zimmermann, U., Rohbock, K., Kopschall, I., Limberger, A., Minichiello, L., and Knipper, M. (2003) *Development* **130,** 4741-4750
23. Engel, J., Braig, C., Ruttiger, L., Kuhn, S., Zimmermann, U., Blin, N., Sausbier, M., Kalbacher, H., Munkner, S., Rohbock, K., Ruth, P., Winter, H., and Knipper, M. (2006) *Neuroscience* **143,** 837-849
24. Combet, C., Jambon, M., Deleage, G., and Geourjon, C. (2002) *Bioinformatics* **18,** 213-214
25. Lim, D. J. (1987) *Hear. Res.* **28,** 9-21
26. Verpy, E., Weil, D., Leibovici, M., Goodyear, R. J., Hamard, G., Houdon, C., Lefevre, G. M., Hardelin, J. P., Richardson, G. P., Avan, P., and Petit, C. (2008) *Nature* **456,** 255-258
27. Thalmann, I. (1993) *Connect. Tissue Res.* **29,** 191-201
28. Deans, M. R., Peterson, J. M., and Wong, G. W. (2010) *PLoS One* **5,** e12765
29. Rau, A., Legan, P. K., and Richardson, G. P. (1999) *J. Comp Neurol.* **405,** 271-280
30. Klaile, E., Vorontsova, O., Sigmundsson, K., Muller, M. M., Singer, B. B., Ofverstedt, L. G., Svensson, S., Skoglund, U., and Obrink, B. (2009) *J. Cell Biol.* **187,** 553-567
31. Goodyear, R. J. and Richardson, G. P. (2002) *J. Neurobiol.* **53,** 212-227
32. Ryan, A. and Dallos, P. (1975) *Nature* **253,** 44-46

33. Zheng, J., Miller, K. K., Yang, T., Hildebrand, M. S., Shearer, A. E., DeLuca, A. P., Scheetz, T. E., Drummond, J., Scherer, S. E., Legan, P. K., Goodyear, R. J., Richardson, G. P., Cheatham, M. A., Smith, R. J., and Dallos, P. (2011) *Proc. Natl. Acad. Sci. U. S. A* **108,** 4218-4223
34. Russell, I. J., Legan, P. K., Lukashkina, V. A., Lukashkin, A. N., Goodyear, R. J., and Richardson, G. P. (2007) *Nat. Neurosci.* **10,** 215-223
35. Legan, P. K., Lukashkina, V. A., Goodyear, R. J., Kossi, M., Russell, I. J., and Richardson, G. P. (2000) *Neuron* **28,** 273-285
36. Verpy, E., Leibovici, M., Michalski, N., Goodyear, R. J., Houdon, C., Weil, D., Richardson, G. P., and Petit, C. (2011) *J. Comp Neurol.* **519,** 194-210
37. Hasko, J. A. and Richardson, G. P. (1988) *Hear. Res.* **35,** 21-38
38. Simmler, M. C., Cohen-Salmon, M., El-Amraoui, A., Guillaud, L., Benichou, J. C., Petit, C., and Panthier, J. J. (2000) *Nat. Genet.* **24,** 139-143
39. Jovine, L., Darie, C. C., Litscher, E. S., and Wassarman, P. M. (2005) *Annu. Rev. Biochem.* **74,** 83-114

Acknowledgements–Continuous support by the animal facilities of the Gene Center and the Walter Brendel Center of Experimental Medicine, Ludwig-Maximilians-University, Munich is acknowledged. We would like to thank Tanja Popp, Birgit Stadlbauer and Beata Rutz for excellent technical assistance, and Kyung-Jin Lee and Alexander Buchner for help with the hearing experiments and statistical analysis, respectively.

FOOTNOTES

This work was partly funded by the FöFoLe program of the Faculty of Medicine, University of Munich and is part of the doctoral theses of Constanze Schäuble, Rosemarie Krupar and Annegret Kamp at the University of Munich.

FIGURE LEGENDS

FIGURE 1: CEACAM16 mRNA is selectively expressed in the cochlea. CEACAM16 transcripts were identified by endpoint (A, C) and real-time RT-PCR (B). CEACAM16 mRNA was found in murine cochleae as well as at lower levels in murine cerebellar and pituitary tissue (n=2; A, B) and in the lateral wall of dissected human inner ears (C). β-actin cDNA was amplified to control intactness of the RNAs (A, C) and for normalization (B). The 604 bp DNA fragment in one of the spiral ganglia cDNA samples corresponds to a product with retained intron and thus is probably derived from contaminating genomic DNA (C). The expected sizes of the PCR products are indicated by arrows.

FIGURE 2: Targeted disruption of the murine *Ceacam16* gene. (A) *Targeting strategy.* Structure of the wild-type allele (top), targeting construct (middle) and recombinant allele (bottom). The 6 exons of *Ceacam16* are shown as boxes with the encoded domains indicated above (color code: exons encoding IgV-like domains, red; IgC-like domains blue). Except for *Bam*HI only restriction endonuclease sites relevant for cloning or probe generation are shown. *Neo* and *tk* expression cassettes which can be used for the selection of homologous recombinants (G418 and gancyclovir resistant) are shown as open boxes. Black arrows indicate the transcriptional direction. The vector sequence within the targeting plasmid is shown as a thin line. The positions and predicted sizes of the DNA fragments obtained after digestion with *Bam*HI and hybridization with the 5′- (blue) and 3′-probes (red), respectively, are indicated. Positions of primers used for identification of ES cell clones with homologous recombination, genotyping and detection of *Ceacam16* transcripts are shown by half arrows. (B) *Identification of targeted ES cell clones by long range PCR.* A total of 3 recombinant ES cell clones could be identified out of 200 clones tested. (C) *Southern blot analysis*. Analysis of DNA from ES cell clones B6, C3 and D1 and from F2 offspring (#97, #98, #152) of a C3-derived chimeric founder after heterozygous mating of F1 mice demonstrated correct recombination events at 3′-region and the 5′-region of the targeted allele of *Ceacam16,*

respectively. Absence and presence of CEACAM16 mRNA and protein was demonstrated in adult (>20 weeks old) *Ceacam16*$^{-/-}$ and *Ceacam16*$^{+/+}$ mice by RT-PCR (D) and Western blotting (E), respectively. As a control, β-actin-specific primers and antibodies were used. The mobility and size of marker DNA fragments and proteins are shown in the left margins. Wild-type (+/+), heterozygous (+/-) and homozygous genotypes (-/-) for the *Ceacam16* knock-out allele are indicated above the lanes.

FIGURE 3: **Hearing function of *Ceacam16*$^{-/-}$ mice.** Young (1-1.4 months old) (A-F) and old *Ceacam16*$^{+/+}$ and *Ceacam16*$^{-/-}$ mice (7-19 month old) (G-L) were analyzed for ABR threshold. Click (A, G) and pure tone stimulation (B, H). Hearing threshold was significantly increased in the low and high frequency hearing range in young *Ceacam16*$^{-/-}$ mice. In aged *Ceacam16*$^{-/-}$ mice threshold increase was detected at the lower frequency range of hearing (2-8 kHz). (C, I) ABR waveform to click stimuli of 85 dB SPL level along 10 ms recording time (upper panel) and waviness of ABR amplitude deflections (derivative, lower panel) as function of stimulation level (dB SPL). ABR waveform upon click stimulation showed the typical waves in young wild-type mice, and similar waveform but reduced amplitudes in young *Ceacam16*$^{-/-}$ mice. ABR amplitude, latencies and waviness are affected by age and are furthermore impaired in the *Ceacam16*$^{-/-}$ mice. In aged mice ABR amplitudes were smaller in wild-type mice and even further reduced in *Ceacam16*$^{-/-}$ mice. Signal derivative reveals similar threshold but reduced ABR signal strength (gain) in the ABR wave of *Ceacam16*$^{-/-}$ mice at suprathreshold stimulation, resulting in a downshift of the curve. Signal derivative for aged *Ceacam16*$^{-/-}$ mice displays a loss of threshold, and loss of suprathreshold gain. Amplitudes (D, J), threshold (E, K), and growth functions (F, L) of the 2f1-f2 distortion product of the otoacoustic emission (DPOAE) were measured for young and old *Ceacam16*$^{+/+}$ and *Ceacam16*$^{-/-}$ mice. Growth function is shown for f2 = 11.3 kHz stimulation with increasing sound pressure (mean ± SE). In young mice, DPOAE threshold was not found to be different (E, and arrowhead in F), but suprathreshold signal amplitudes fell behind the values for wild-type mice, indicating reduced coupling of force by OHC motility into the cochlear amplifier. DPOAE amplitudes were still significantly decreased for aged *Ceacam16*$^{-/-}$ mice as compared to wild-type mice and many individuals had amplitudes dropped to nearly noise level (open circles clustered at ca. -10 dB SPL 2f1-f2 amplitude, J, encircled). OHC amplification loss in aged *Ceacam16*$^{-/-}$ mice became evident from the 2f1-f2 threshold audiogram (K) and from the DPOAE growth function (L). Black symbols in E and K are slightly horizontally displaced for better visualization. Statistical significance of differences was tested by t-test (click, 2f1-f2 max) or 2-way ANOVA with post hoc t-test (tone burst, 2f1-f2 growth). Significance levels are given in the graph with $p<0.05$ (*), $p<0.01$(**) and $p<0.001$(***). Small symbols in A, D, G and J show values for single ears. The numbers (n) of ears analyzed are indicated. Mean ± SD or ± SE (L, 21-f2 growth).

FIGURE 4: Progression of age-related hearing loss. ABR threshold to click stimuli was measured in aging *Ceacam16*$^{+/+}$ and *Ceacam16*$^{-/-}$ mice, 1-19 months of age. Individual ear threshold (dB SPL) was correlated to age (months). Continuous lines show a linear fit. Pearson Product-Moment Correlation Coefficient (R^2) and significance of correlation is given close to the line fit. For both *Ceacam16*$^{+/+}$ and *Ceacam16*$^{-/-}$ mice, loss of ABR hearing threshold showed a similar progression with age. Nevertheless the threshold for *Ceacam16*$^{-/-}$ mice was continuously significantly higher.

FIGURE 5: Expression of CEACAM16 in the cochlea and vestibular organ. Expression of CEACAM16 was analyzed in the cochleae and vestibular organ of *Ceacam16*$^{+/+}$ (A-C, I, J) and *Ceacam16*$^{-/-}$ mice (E-G) by immunohistology using the biotinylated monoclonal anti-human CEACAM16 antibody 9D5 which cross-reacts with murine CEACAM16. CEACAM16 (brown stain) was observed in the acellular TM (A, B, I, J) and in the extracellular matrix covering the macula cells of the saccule (C) in wild-type, but not in *Ceacam16*$^{-/-}$ mice. Furthermore, staining for CEACAM16 was observed in interdental cells in the helicotremal region of P15 wild-type cochleae (I) and also in adult *Ceacam16*$^{+/-}$ mice (J). No staining was seen when only horseradish peroxidase-coupled streptavidin was added (K). Comparable staining for α-tectorin was found in the TM in both *Ceacam16*$^{+/+}$ (D) and *Ceacam16*$^{-/-}$ mice (H). The age of the mice (days *post partum*) is indicated at the lower left corners. Note that the TM of *Ceacam16*$^{-/-}$ mice is significantly more often in contact with the OHC (E, F, H) whereas it is either

detached or more retracted in wild-type mice (B, D, I, J). No difference was observed when different regions of the cochlea (base, medal region or helicotrema-proximal) were analyzed. Five wild-type and 4 *Ceacam16*$^{-/-}$ mice, representing 8 and 7 cochleae, respectively, were evaluated; p = 0.0003, Fisher's exact test (L). B, basilar membrane; GER, greater epithelial ridge; ID, interdental cells; IHC, inner hair cell; IS, inner sulcus; M, macula; OHC, outer hair cells; R, Reissner's membrane; SV, *stria vascularis*; SL, spiral limbus; TM, tectorial membrane.

FIGURE 6: Postnatal expression of CEACAM16 in the organ of Corti. Expression of CEACAM16 was analyzed in the cochleae of *Ceacam16*$^{+/+}$ mice 5-18 days *post partum* (P5-P18) by immunohistology using the monoclonal anti-human CEACAM16 antibody 9D5 (A-C, G-I). As negative control, cochleae of *Ceacam16*$^{-/-}$ mice were analyzed (D-F, J-L). CEACAM16 (brown stain) was observed in the TM starting at P12 and continued to be present in P18 mice. Note the preferential staining at the marginal band (MB) and limbal zone (LZ) and the sulcus proximal part of the medial zone (MZ) of the TM (arrowhead) in P12 and lack of staining in the middle part. In P15 and P18 mice homogenous staining for CEACAM16 was found (H, I). In P12, P15 and P18 cochleae CEACAM16 was present also in OHC, Deiters cells and in interdental cells (G-I, arrows). Magnification bar: 50 µm. The appearance of immunoreactive CEACAM16 protein in cochlear tissues is preceded by *Ceacam16* mRNA expression detectable from P10 onward with a maximum around P13, a time point, where only marginal amounts of α-tectorin (*Tecta*) and stereocilin (*Strc*) mRNA are found by qRT-PCR. Note continued expression of *Ceacam16* into adulthood which is not observed for *Tecta* and *Strc* (M). GER, greater epithelial ridge; D1, D2, Deiters cell 1, 2; ID, interdental cells; IS, inner sulcus; L, limbus; LZ, limbal zone; MB, marginal band; MZ, medial zone; OHC, outer hair cells; R, Reissner's membrane; TM, tectorial membrane.

FIGURE 7: CEACAM16 is expressed in Deiters cells. Expression of CEACAM16 was analyzed in the organ of Corti of adult (P49) *Ceacam16*$^{+/+}$ (A-F, G, H) and 44 weeks old *Ceacam16*$^{-/-}$ mice (A, inset) by immunofluorescence using the monoclonal anti-CEACAM16 antibody 9D5. CEACAM16 (red color) was observed in the OHC-supporting Deiters cells (A, C, D, F, H) which were identified by the potassium channel protein anti-KIR4.1 antibody (green) but not in OHCs which were specifically identified by anti-prestin antibodies (green). The shape of OHCs was outlined by stippled lines (C). No CEACAM16 staining could be detected in *Ceacam16*$^{-/-}$ mice (A, inset). Note staining for CEACAM16 in both the cell body and projections of the Deiters cells (open arrows in A, D) which extent to the reticular lamina (arrows in C), the stiff cover of the organ of Corti. The locations of the Deiters cell nuclei are indicated by full arrows (B, D). Nuclei were stained with DAPI (blue). Furthermore, staining for CEACAM16 was observed in the supranuclear (neck) region of IHC (outlined by stippled line) and in pillar cells (G, H). Pillar cells were identified by staining with anti-KIR4.1 antibody. Schematic representation of OHC and Deiters cells is shown in (I). Magnification bars: 10 µm. BM, basilar membrane; DC, Deiters cell; DP, Deiters cell projection; IHC, inner hair cell; OHC, outer hair cells; PC, pillar cell; RL, reticular lamina; SC, stereocilia.

FIGURE 8: Ceacam16 mRNA is expressed in interdental and Deiters cells. Expression of Ceacam16 in the organ of Corti of young rats (P12) was analyzed by *in situ* hybridization of cochlear sections with a Ceacam16 antisense probe. Strong expression of Ceacam16 mRNA (brown color) appears in interdental cells of the limbus (A) and in Deiters cells and to a lesser extent in phalangeal, border, pillar and inner hair cells (B). The shape of the inner and outer hair cells is indicated by broken lines. No specific staining was observed with the sense probe (insets in A and B). (C) Schematic representation of Ceacam16 mRNA expression with color coded expression levels (green, weak expression; blue, strong expression). BM, basilar membrane; BC, border cell; DC, Deiters cell; DP, Deiters cell projection; HC, Hensen's cell; ID, interdental cell; IHC, inner hair cell; IPC, inner pillar cell; ISC, inner sulcus cell; L, limbus; OHC, outer hair cells; OPC, outer pillar cell; PH, phalangeal cell; SC, stereocilia.

FIGURE 9: CEACAM16 interacts homotypically. HEK293T cells either remained untransfected (A) or were transiently transfected with expression plasmids encoding full-length murine native (B) or GPI-

linked CEACAM16 (C). The transfected cells were harvested by repeated pipetting, incubated at room temperature, attached to glass slides using the cytospin method and stained with anti-murine CEACAM16 immune sera by immunocytochemistry (brown stain). Note homotypic sorting of cells expressing CEACAM16 on the cell membrane (C), but not of cells with intracellular expression (B). This suggests that CEACAM16 can interact homotypically in trans. Aggregation of HEK293T cells was tested as above after transient expression of GPI-anchored human CEACAM16 N1 and N2 domains (D, E left panels). N1- and N2-expressing cells were detected by immunocytochemistry using an anti-myc-tag antibody. Representative regions of the cytospins are shown. The expression levels of myc-tagged fusion proteins and the fraction of positive cells were determined by FACScan analysis using anti-myc and FITC-conjugated secondary antibodies (D, E right panels, green curves). Samples incubated without primary antibody served as a negative control (blue curves). Aggregation mediated by N1 and N2 domains was quantitated by determination of the fraction of N1- and N2-positive cells, respectively, in single and doublet cell populations as well as in aggregates ≥ 3 using the cytospins shown in D and E (F). Note that surface expression of N2 preferentially induces multicellular aggregates. One of two experiments with similar results is shown. Full-length murine native CEACAM16 (G) or a deletion constructs lacking N2 (H) or N1 and A (J) or B and N2 (K) or encoding only the N1 or N2 domain either soluble (I, upper panel) or GPI-linked (I, lower panels), were expressed in HEK293T cells by transient transfection. Cell lysates (cells) or cell culture supernatants with or without prior treatment with DTT were separated by gel electrophoresis and CEACAM16 was detected by Western blot analysis with a monoclonal anti-myc antibody. The domain organization of the encoded proteins is schematically shown to the right. Cysteines possibly involved in intermolecular disulfide bridges are indicated by yellow dots, green tags represent N-terminally added myc epitopes and green arrows symbolize GPI anchors. Presumed monomeric, dimeric and oligomeric forms of CEACAM16 are indicated by arrows. Note that the N2 or the N1 and A domains appear to be dispensable for interaction since dimers are observed in the absence of these domains (J). The 60 kDa band which is observed in the supernatant of transfected and mock transfected cells is marked by an asterisk (H, J, K).

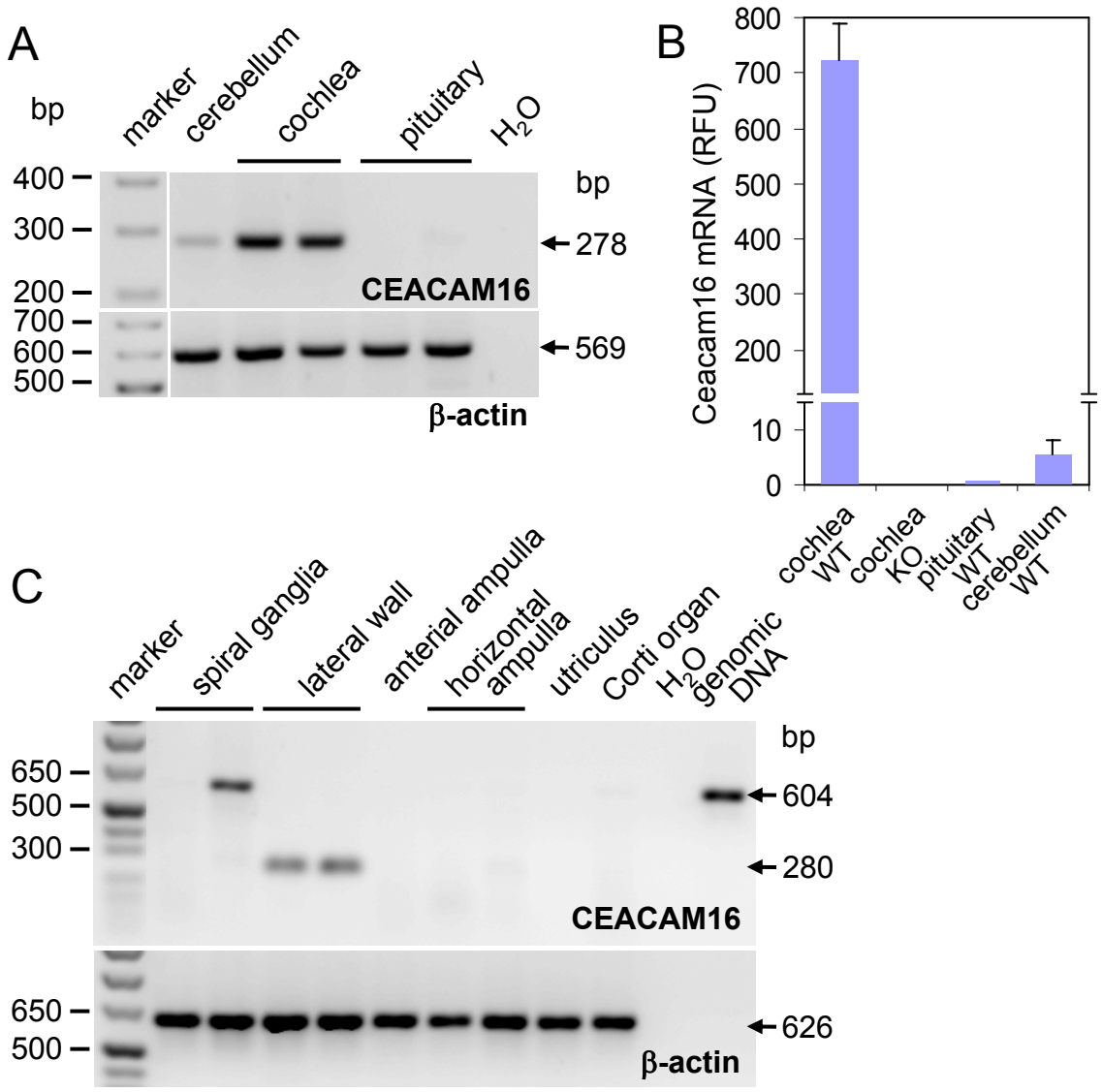

Figure 1

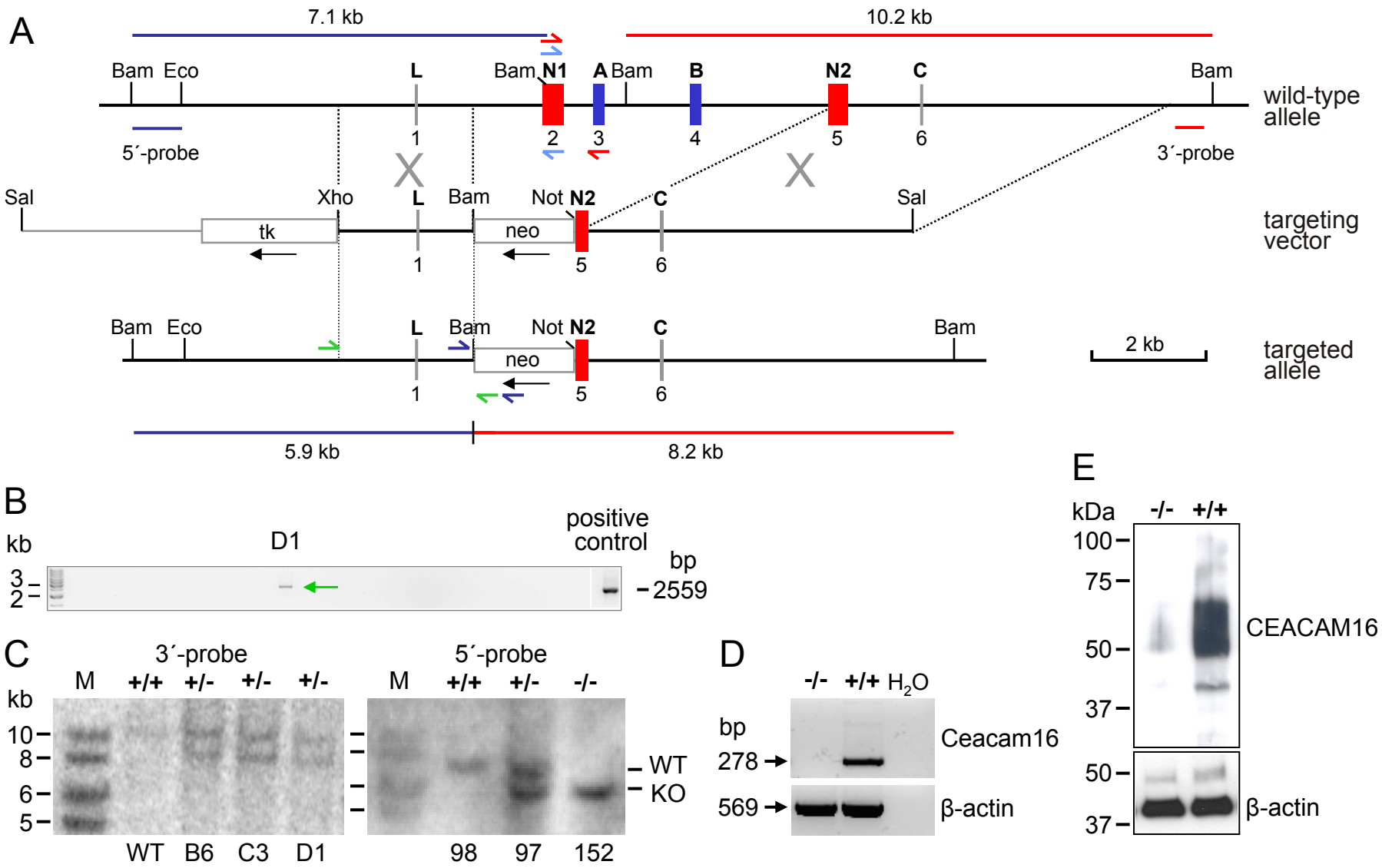

Figure 2

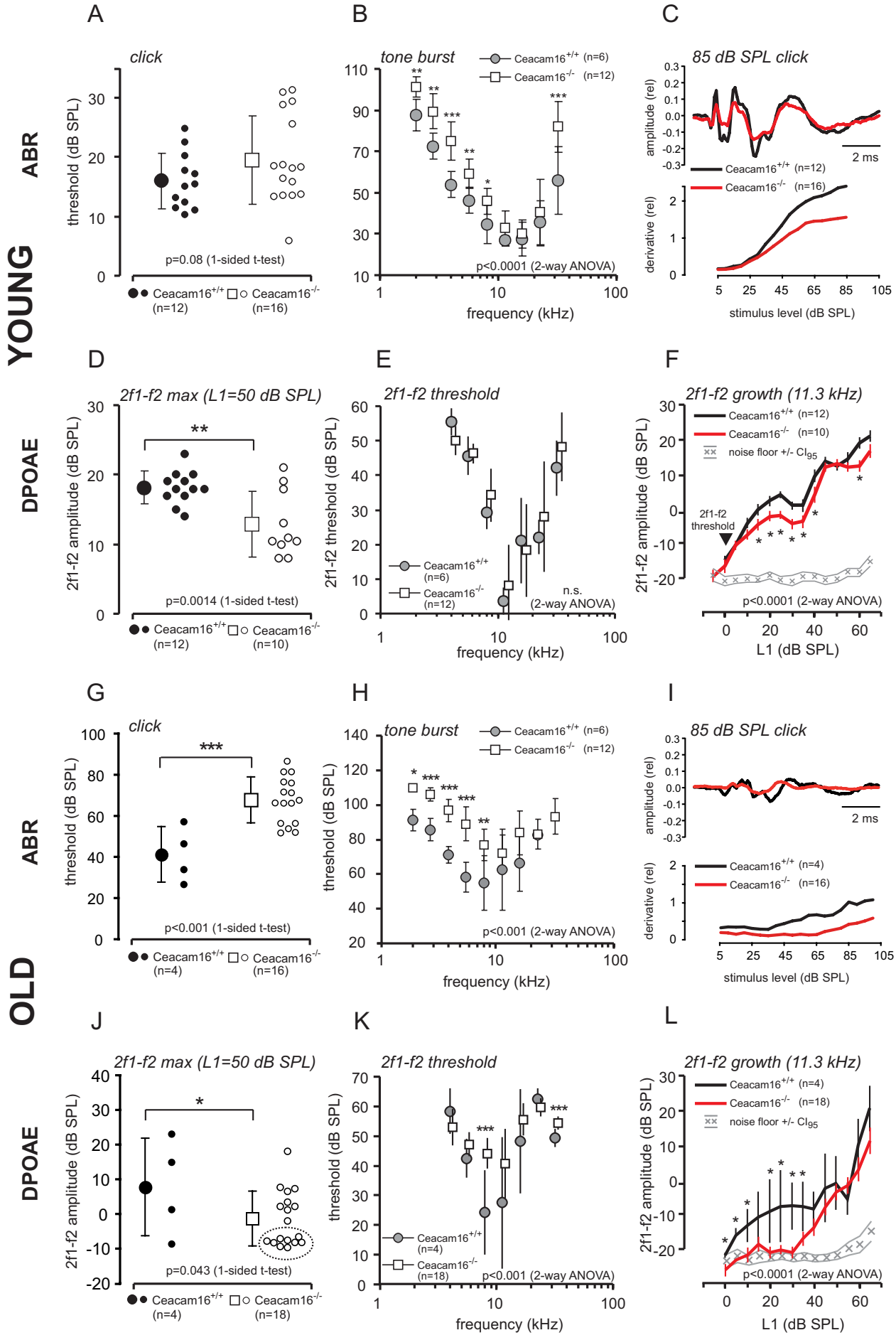

Figure 3

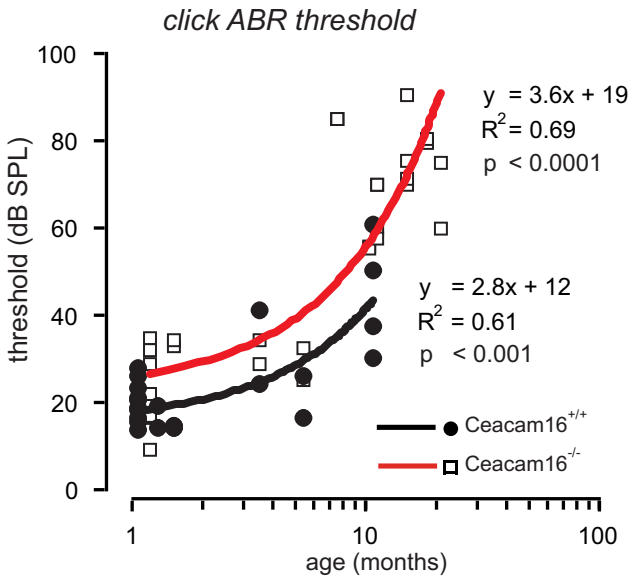

Figure 4

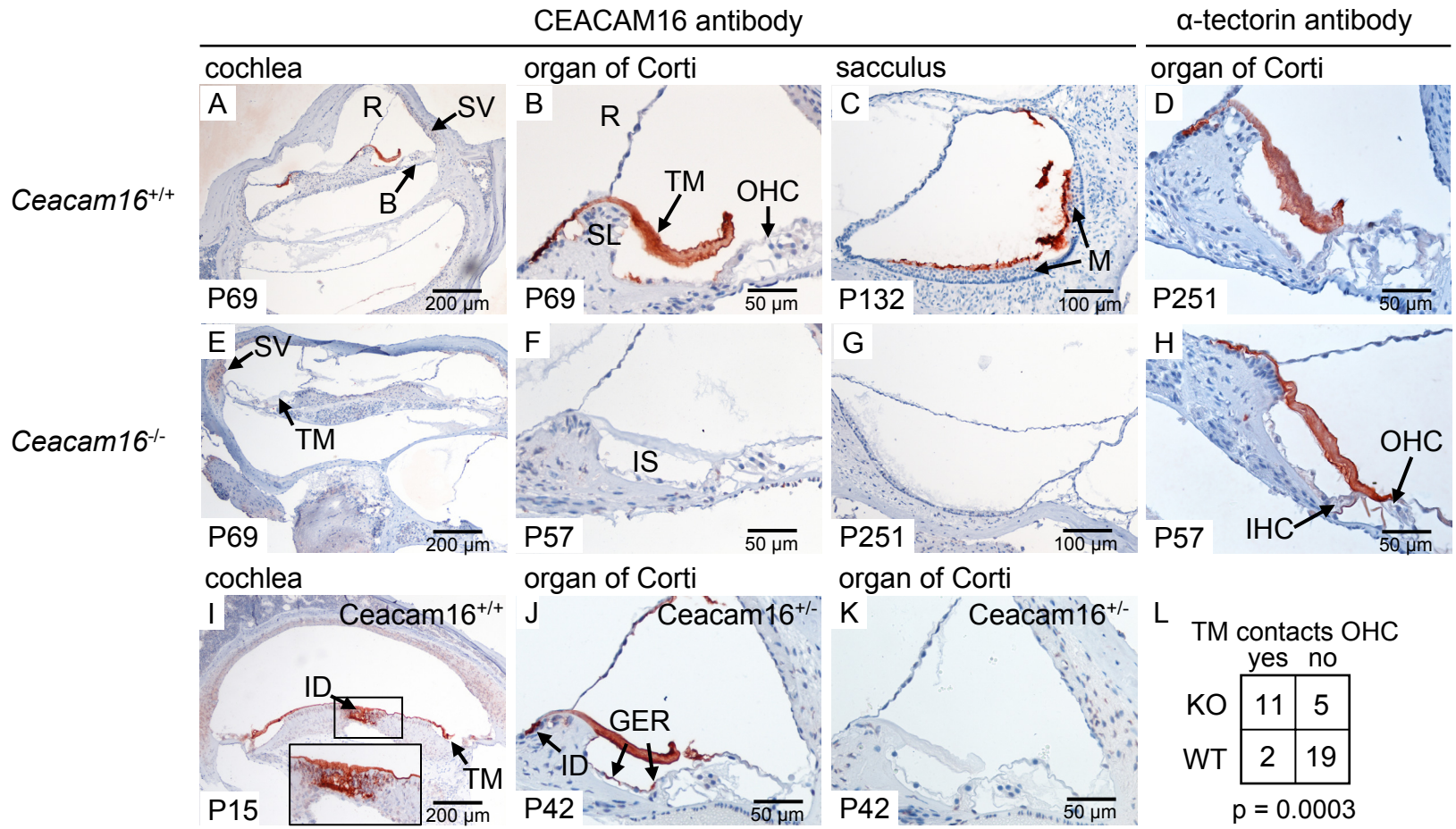

Figure 5

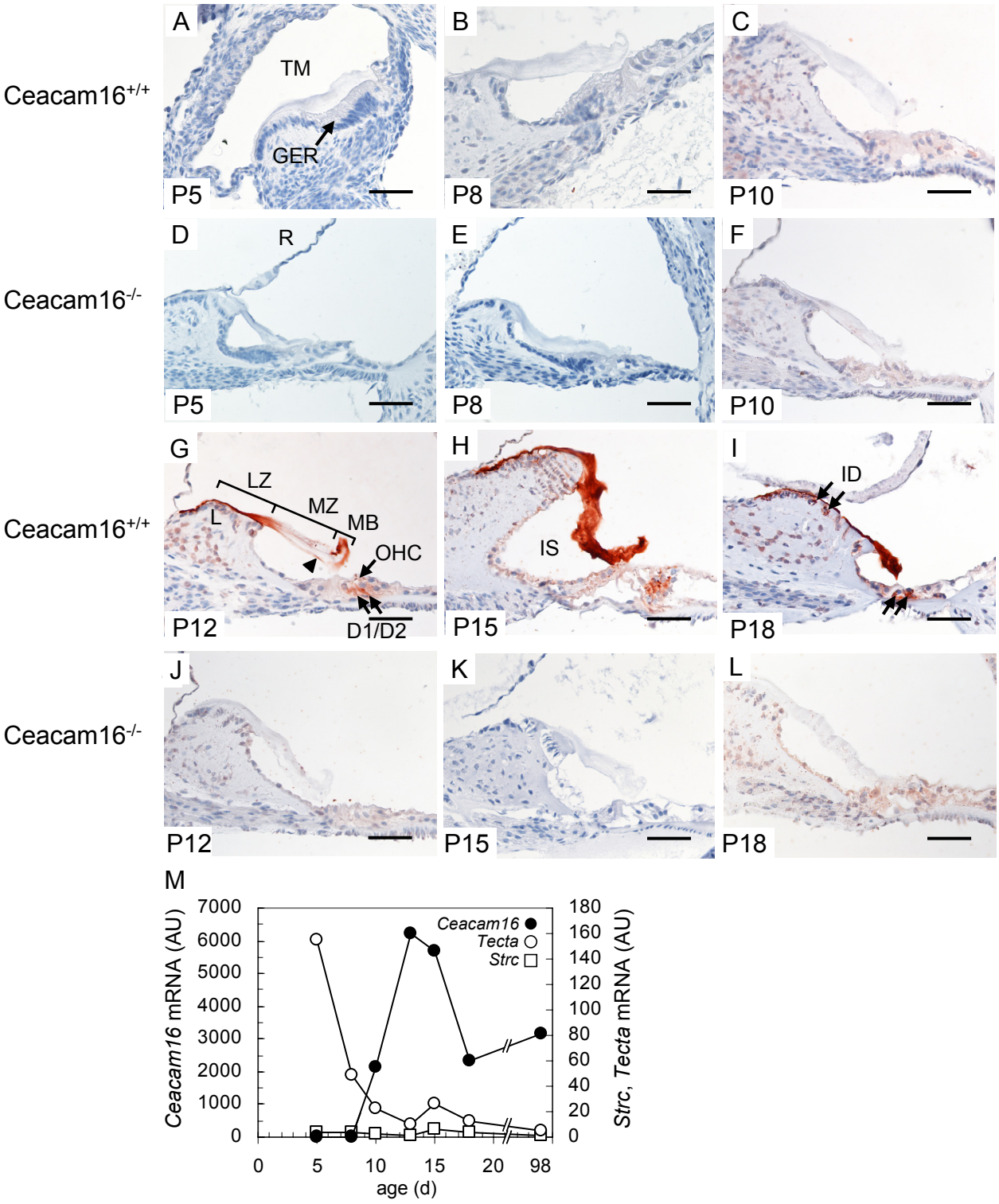

Figure 6

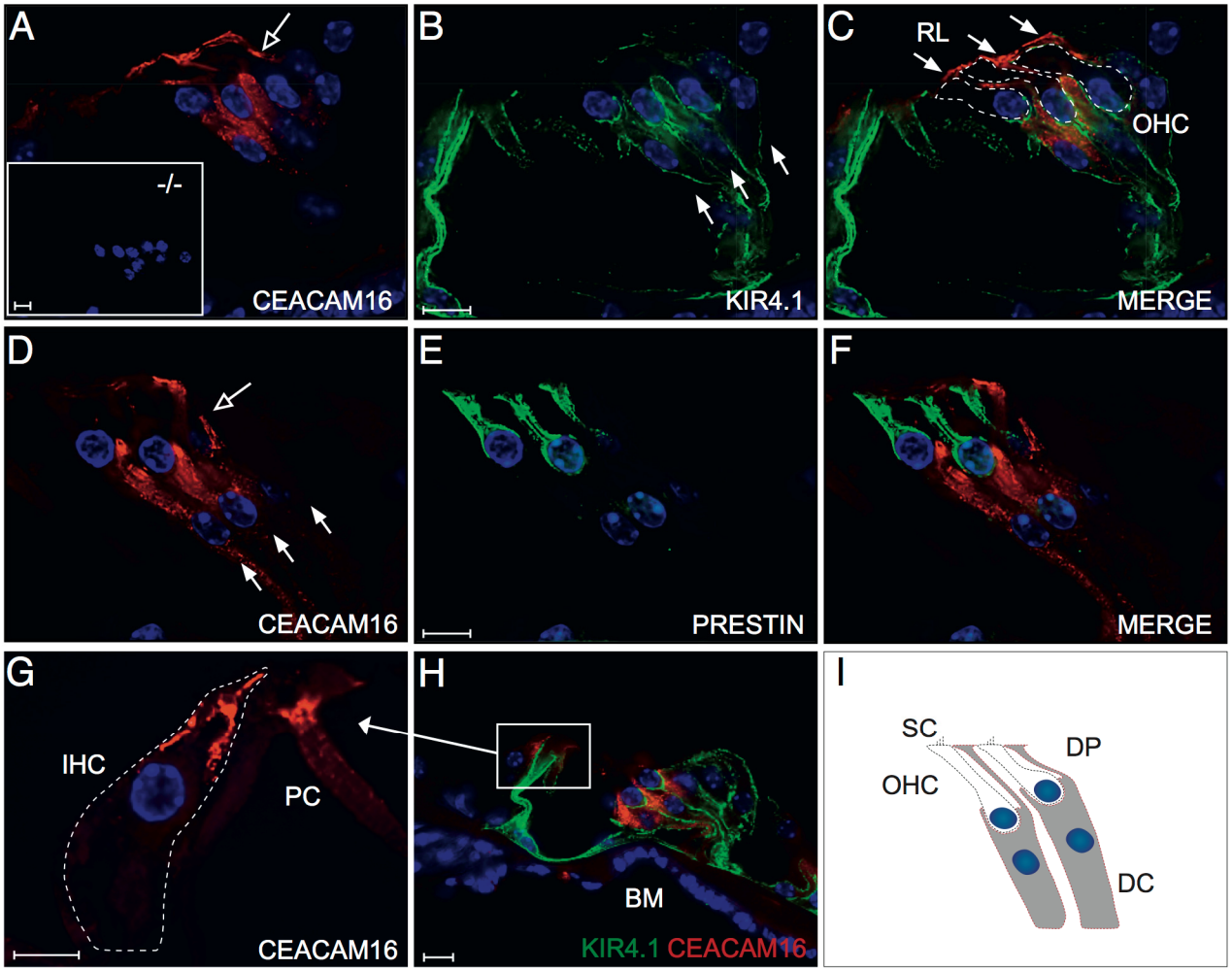

Figure 7

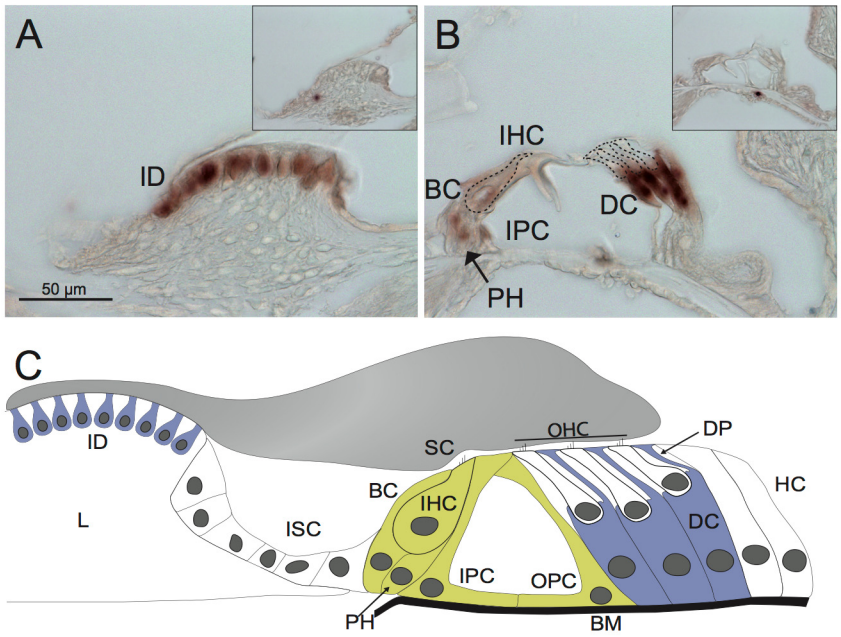

Figure 8

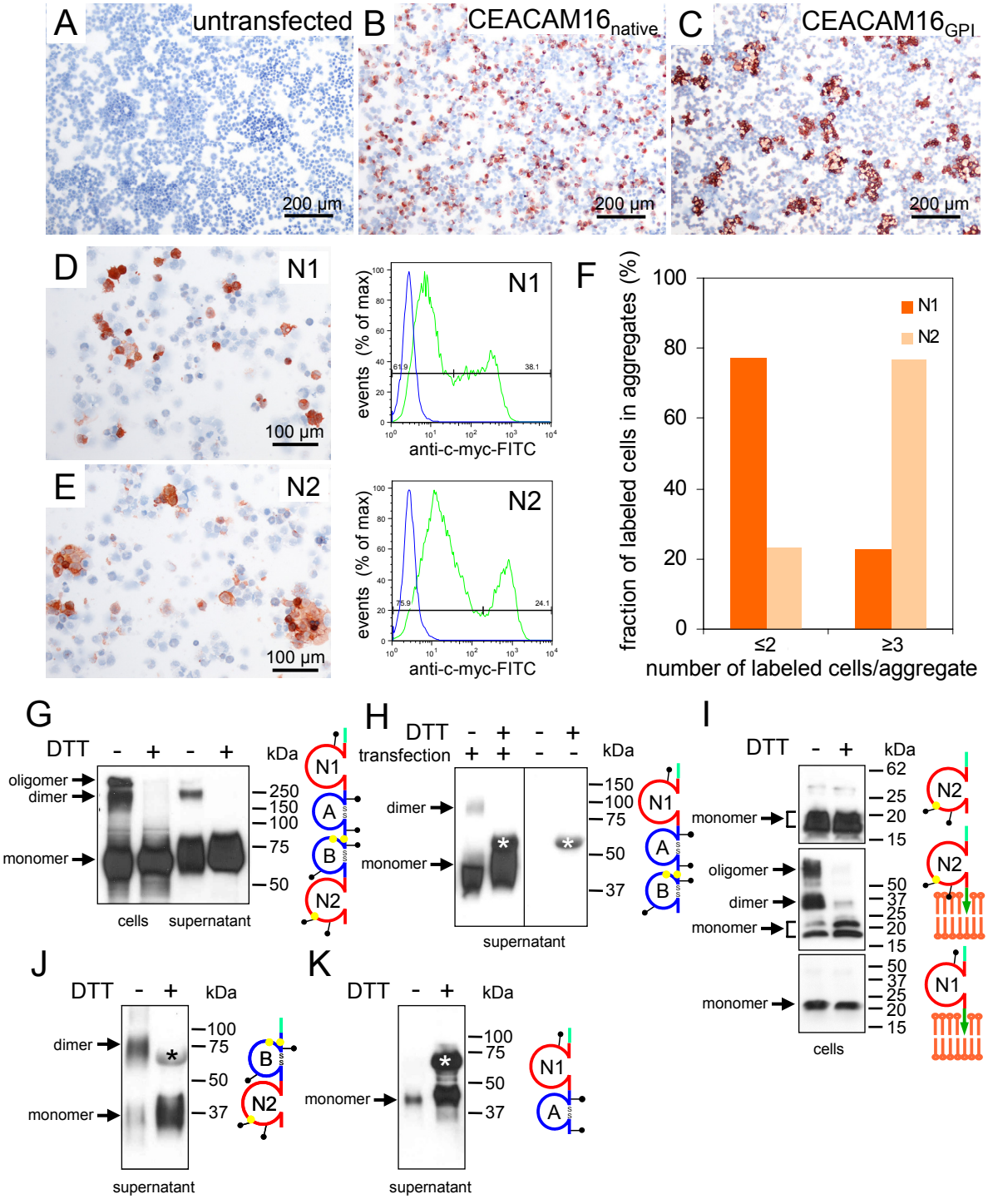

Figure 9